ESC European Society of Cardiology
Cardiovascular Research
doi:10.1093/cvr/cvz291

Myocardial overexpression of ANKRD1 causes sinus venosus defects and progressive diastolic dysfunction

Nicoletta Piroddi[1], Paola Pesce[2], Beatrice Scellini [1], Stefano Manzini [3], Giulia S. Ganzetti[3], Ileana Badi [4†], Michela Menegollo [5], Virginia Cora[5], Simone Tiso[5], Raffaella Cinquetti [4], Laura Monti [4], Giulia Chiesa[3], Steven B. Bleyl[6], Marco Busnelli [3], Federica Dellera[3], Daniele Bruno[4], Federico Caicci[7], Annalisa Grimaldi [4], Roberto Taramelli[4], Lucia Manni [7], David Sacerdoti [2], Chiara Tesi[1], Corrado Poggesi[1], Simonetta Ausoni [5]*, Francesco Acquati [4]*, and Marina Campione [5,8]*

[1]Department of Experimental and Clinical Medicine, University of Florence, 50134 Florence, Italy; [2]Department of Medicine, University of Padua, 35121 Padua, Italy; [3]Department of Pharmacological and Biomolecular Sciences, University of Milan, 20133 Milan, Italy; [4]Department of Biotechnology and Life Sciences, University of Insubria, 21100 Varese, Italy; [5]Department of Biomedical Sciences, University of Padua, 35121 Padua, Italy; [6]Department of Pediatrics, University of Utah, Salt Lake City, 84132 UT, USA; [7]Department of Biology, University of Padua, 35121 Padua, Italy; and [8]CNR-Neuroscience Institute, 35121 Padua, Italy

Received 4 March 2019; revised 26 September 2019; editorial decision 26 October 2019; accepted 30 October 2019

Time for primary review: 39 days

Aims Increased Ankyrin Repeat Domain 1 (ANKRD1) levels linked to gain of function mutations have been associated to total anomalous pulmonary venous return and adult cardiomyopathy occurrence in humans. The link between increased ANKRD1 level and cardiac structural and functional disease is not understood. To get insight into this problem, we have generated a gain of function ANKRD1 mouse model by overexpressing ANKRD1 in the myocardium.

Methods and results Ankrd1 is expressed non-homogeneously in the embryonic myocardium, with a dynamic nucleo-sarcomeric localization in developing cardiomyocytes. ANKRD1 transgenic mice present sinus venosus defect, which originates during development by impaired remodelling of early embryonic heart. Adult transgenic hearts develop diastolic dysfunction with preserved ejection fraction, which progressively evolves into heart failure, as shown histologically and haemodynamically. Transgenic cardiomyocyte structure, sarcomeric assembly, and stability are progressively impaired from embryonic to adult life. Postnatal transgenic myofibrils also present characteristic functional alterations: impaired compliance at neonatal stage and impaired lusitropism in adult hearts. Altogether, our combined analyses suggest that impaired embryonic remodelling and adult heart dysfunction in ANKRD1 transgenic mice present a common ground of initial cardiomyocyte defects, which are exacerbated postnatally. Molecular analysis showed transient activation of *GATA4-Nkx2.5* transcription in early transgenic embryos and subsequent dynamic transcriptional modulation within titin gene.

Conclusions ANKRD1 is a fine mediator of cardiomyocyte response to haemodynamic load in the developing and adult heart. Increased ANKRD1 levels are sufficient to initiate an altered cellular phenotype, which is progressively exacerbated into a pathological organ response by the high ventricular workload during postnatal life. Our study defines for the first time a unifying picture for ANKRD1 role in heart development and disease and provides the first mechanistic link between ANKRD1 overexpression and cardiac disease onset.

* Corresponding authors. Tel: +39 049 8276036; fax: +39 049 8276040, E-mail: simonetta.ausoni@unipd.it (S.A.); Tel: +39 0332 421512; fax: +39 0332 421500, E-mail: francesco.acquati@uninsubria.it (F.A.); Tel: +39 049 8276031; fax: +39 049 8276040, E-mail: campione@bio.unipd.it (M.C.)

† Present address. Division of Cardiovascular Medicine, Radcliffe Department of Medicine, University of Oxford, John Radcliffe Hospital, Oxford OX3 9DU, UK.

Keywords ANKRD1 • Sinus venosus congenital heart defect • Diastolic dysfunction • Cardiomyocyte structure and contractility • Titin

Graphical Abstract

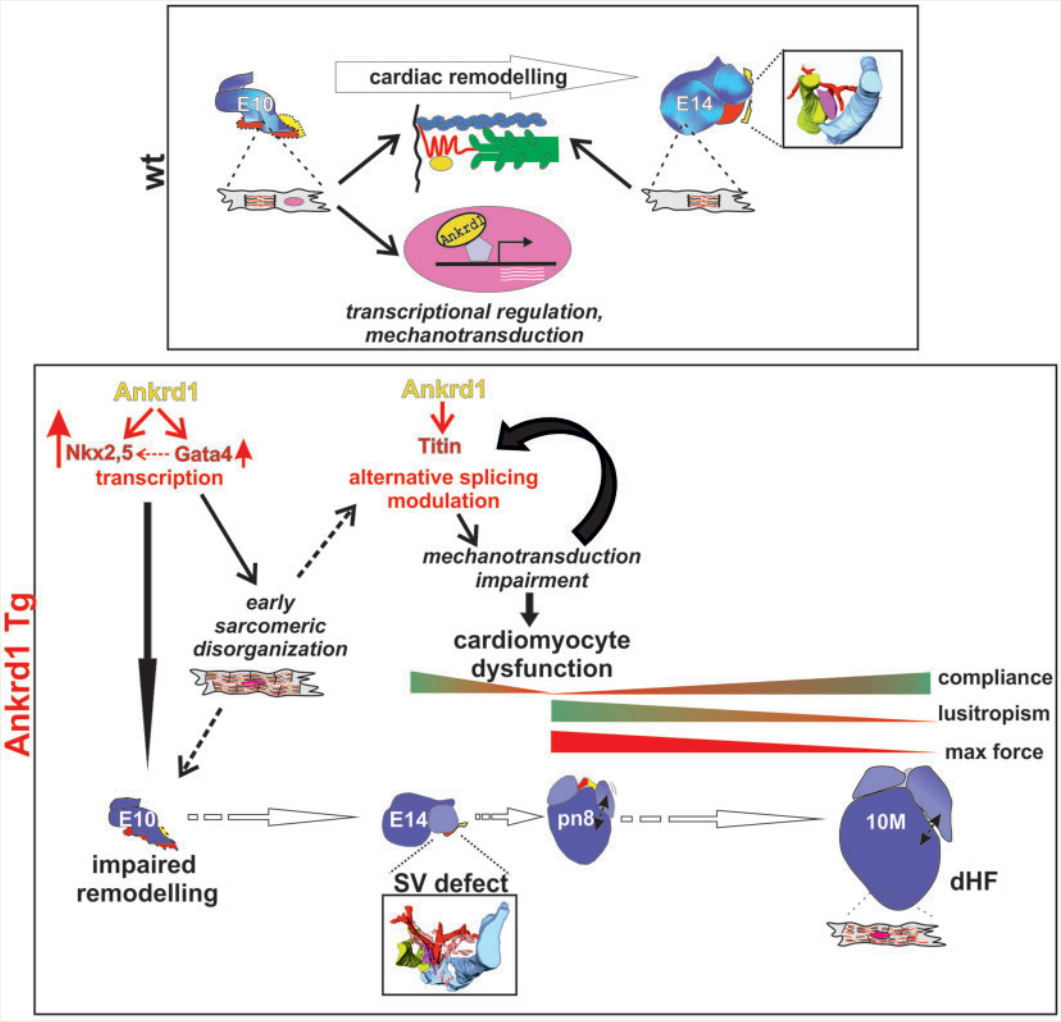

1. Introduction

Ankyrin Repeat Domain 1 (ANKRD1, also known as Cardiac Ankyrin Repeat Protein, CARP) is a member of the muscle-specific ankyrin repeat proteins (MARP) family, which also includes ANKRD2/Arpp and DARP.[1,2] MARP proteins are involved in muscle stress response and are structurally characterized by four ankirin repeats, a coiled-coil domain, a nuclear localization signal, and a PEST degradation sequence, which mediates its rapid turnover via the ubiquitin-proteasome pathway.[3,4]

ANKRD1 is highly expressed during heart development and down-regulated in adult life.[5–7] In the developing heart, ANKRD1 has been proposed to work as transcriptional cofactor and negative regulator of myocardial gene expression.[5–7] ANKRD1 is a target of Nkx2.5 *in vivo*[5] and its promoter can be cooperatively activated by Nkx2.5 and GATA4.[6]

In adult cardiomyocytes, ANKRD1 is normally located at the sarcomere, but it has been shown to translocate to the nucleus upon mechanical stimulation *in vitro*.[2] In the sarcomere, ANKRD1 is found at the I-band where it is a component of titin N2A-linked signalling complex.[2,8] Physical interaction between ANKRD1 and titin N2A spring domain has been shown to reduce PKA phosphorylation and titin compliance.[1] ANKRD1 has additionally been shown to functionally interact with GATA4 in the I band and the nucleus, thereby modulating GATA4-mediated sarcomeric gene expression and sarcomeric organization.[9,10] Interactions with several additional partners involved in modulation of muscle structure and function have been reported.[3,8] ANKRD1 is therefore part of a stretch-sensing unit capable of relaying biomechanical stress signals to the regulation of gene expression. In line, ANKRD1 expression is up-regulated in response to hypertrophy and in heart failure (HF).[6,11–13] However, the absence of cardiac phenotype in ANKRD1 knock-out mouse models,[10,14] combined with contradictory results from loss and gain of function approaches,[3,9,15,16] have precluded a clear understanding of ANKRD1 role in adult heart.

Genetic mutations in *ANKRD1*, mostly associated to a gain of function condition, have been correlated to several types of cardiac disease in humans. *ANKRD1* missense mutations have been identified in patients with hypertrophic and dilated cardiomyopathy (HCM, DCM).[17–19] *ANKRD1* has additionally been identified as a candidate gene for total anomalous pulmonary venous return (TAPVR) in isolated patients.[20,21] TAPVR is a congenital heart disease (CHD) which affects 1:15 000 live births and is characterized by incorrect pulmonary vein (PV) drainage into the heart.[22] TAPVR leads to high mortality rate in the first year of life, unless surgically corrected. Reported TAPVR patients presented either chromosomal rearrangement or T116M–*ANKRD1* mutation, leading respectively to a three- to four-fold increase in *ANKRD1* transcript levels or 10–20% increase in protein stability,[4,21] suggesting that *ANKRD1* expression levels must be tightly regulated during embryogenesis.

Here, we show that Ankrd1 is heterogeneously expressed in the developing heart, with a dynamic nucleo-sacroplasmic sublocalization. Myocardial-overexpressing ANKRD1 transgenic (Tg) mice are born with congenital sinus venosus (SV) defect. In postnatal life, diastolic dysfunction and progressive transition from adaptive to maladaptive response occurs. Increased ANKRD1 levels are sufficient to initiate an altered cellular phenotype in the embryonic heart, which is exacerbated postnatally by high ventricular workload.

2. Methods

2.1 Mouse lines

Human wt-ANKRD1-FLAG tagged cDNA[4] was cloned downstream of the 5 kb *Myh6* promoter.[23] Two Tg lines were generated by pronuclear microinjection of linearized constructs into FVB oocytes. Transgene expression was characterized by western blotting and immunofluorescence (Supplementary material online, *Figure S1*). Genomic DNA was PCR-genotyped from tails of anaesthetized mice (Zoletil, 30 mg/kg, i.p) or the amniotic sac of embryos isolated after sacrifice by cervical dislocation of the anaesthetized mother. Isolated embryos, neonatal, and adult hearts were isolated and processed using standard procedures for subsequent histological, biochemical, or molecular analysis. Animal procedures used conformed to the guidelines from Directive 2010/63/EU of the European Parliament on the protection of animals used for scientific purposes.

2.2 PCR analysis

RNA isolation, cDNA transcription, and quantitative PCR were conducted using standard procedures. Primers for titin PCR amplification were selected to avoid regions with repetitive nucleotide sequences and potential incorrect priming. All primer sequences are available in Supplementary material online, *Table S1*.

2.3 Isolated myofibril analysis

Myofibrils were prepared by homogenization of permeabilized strips of frozen ventricular tissue in relaxing solution on ice.[24] Mechanical measurements from myofibrils in isometric conditions were performed during activation-relaxation cycles achieved by fast solution switching.[25] SL-resting tension relations were determined as previously described.[26]

2.4 Echocardiographic analysis

Transthoracic echocardiography was performed using a high-resolution echo machine with a 30 Mhz probe (VEVO 2100 Visualsonics). Both males and females mice were analysed. Mice were chest shaved and anaesthetized with 3% isoflurane, and temperature controlled anaesthesia was maintained with 1.5% isoflurane. Two-dimensional cine loops and M-mode cine loops of a long-axis view and a short-axis view of the left ventricle (LV) were recorded. Interventricular septum thickness, left ventricular internal diameter, and left ventricular posterior wall thickness were measured in diastole and systole from M-mode long-axis view. Ejection fraction (EF) and fractional shortening (FS) were automatically calculated by the machine software.

2.5 Doppler analysis of left ventricular and PV flow

Doppler analysis of left ventricular flow was performed from the long-axis B-mode image placing the sample volume in the left ventricle, below the mitral annulus. Isovolumetric contraction and relaxation times (IVCT, IVRT) and ejection time (ET) were measured from transmitral Doppler analysis. Myocardial performance index was calculated using the following formula: MPI = IVCT+IVRT/ET. E wave, A wave, and E wave deceleration time (DT) were measured from transmitral Doppler flow profile.

Doppler analysis of PV flow was performed from a corrected long-axis B-mode image placing the sample volume just before the entry of the PV in the left aria (Supplementary material online, *Figure S2*). The maximal velocity of PV atrial (a), systolic (s), and diastolic (d) flow waves were measured.

2.6 Statistical analysis

Data are presented as mean ± standard deviation. Comparisons between groups were performed by Students unpaired *t*-test, Mann–Wilcoxon W test, or Wilcoxon signed-rank test where appropriate, based on experimental design. $P < 0.05$ was considered statistically significant.

Detailed methods are available in Supplementary data online.

3. Results

3.1 Ankrd1 is heterogeneously expressed in the developing myocardium

We initially examined *Ankrd1* expression in embryonic hearts. *In situ* hybridization (ISH) on sections showed that *Ankrd1* mRNA is expressed in the myocardium from E7.5 onwards, although not homogeneously (*Figure 1A*).

At the venous pole of the heart, at E10.0 differential *Ankrd1* mRNA levels were observed at the left and right pulmonary ridge and the sinus horns (white arrows, *Figure 1Bb*). By E10.5, heterogeneous mRNA staining was visible also within the developing septum primum (black arrow, *Figure 1Bd*), around the PV (white arrowhead, *Figure 1Bd*) and systemic veins entrance (red arrowheads, *Figure 1Ac* and *Bd*). This expression profile was maintained at E12.5 (*Figure 1Ad* and *1Be, f*) and E14.5 (*Figure 1Bg, h*).

Heterogeneous *Ankrd1* mRNA expression was detected also within the compact and trabecular layers of the left and right atrial chambers (LA, RA) (green arrows, *Figure 1Cb,* e), and the atrioventricular canal (red asterisk, *Figure 1Bh* and *Ce*). Stronger *Ankrd1* expression was visible in the outflow tract and the right ventricle (*Figure 1Ac–e*), whereas weaker and more heterogeneous expression was detected in the LV and the interventricular septum (yellow arrows, *Figure 1Ac, d* and *Cd, f*).

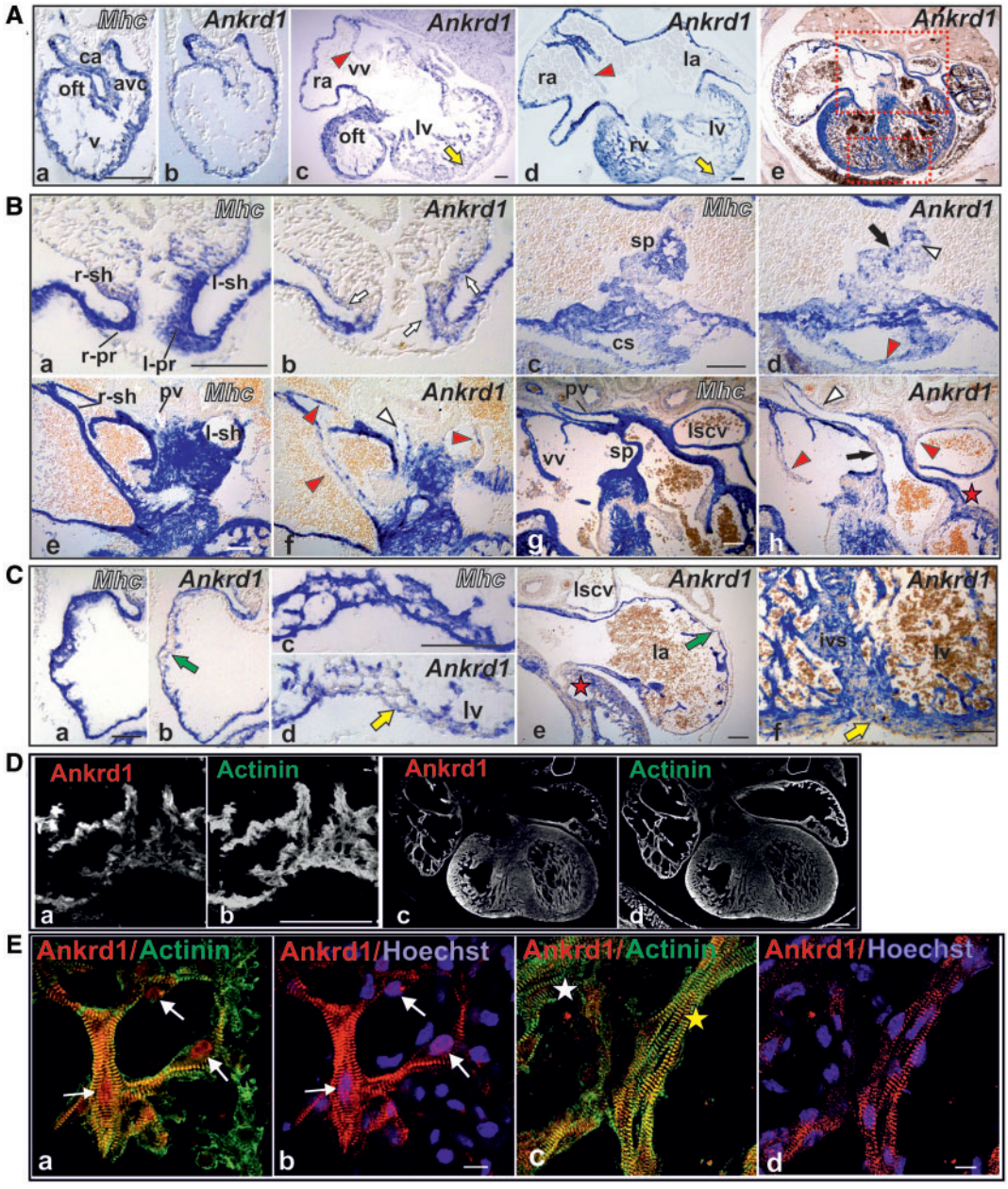

Figure 1 *Ankrd1* mRNA and protein expression in cardiac development. (*A–C*) *Ankrd1* mRNA expression in E8.5–E14.5 hearts, ISH analysis. Myocardium is identified by *Mhc* transcripts. (*A*) E8.5 (*a*, *b*), E10.5 (*c*), E12.5 (*d*), E14.5 (*h*) hearts, global view. Dotted areas in e are magnified below. (*B*) *Ankrd1* expression at venous pole of E10 (*a*, *b*), E10.5 (*c*, *d*), E12.5 (e, *f*), E14.5 (*g*, *h*) embryos. (*C*) *Ankrd1* expression in atrial and ventricular chambers of E10.5 (*a–d*) and E14.5 (e, *f*) embryos. (*D* and *E*) Ankrd1 protein expression and sub-cellular localization in E10.5 and E14.5 hearts, double immunofluorescence and confocal analysis. (*D*) E10.5 (*a*, *b*) and E14.5 (*c*, *d*) hearts, overview pictures. Note heterogeneous reaction of α-Ankrd1 (*a*, *c*) vs. α-actinin (*b*, *d*) antibody. (*E*) At E10.5 (*a*, *b*) Ankrd1 presents sarcomeric and nuclear (arrows) co-localization; at E14.5 (*c*, *d*) Ankrd1 is exclusively sarcomeric. Note strong (yellow star) or low (white star) α-Ankrd1 antibody reaction in neighboring cardiomyocytes. avc, atrioventricular canal; ca, common atrium; icv, inferior caval vein; ivs, interventricular septum; lscv, rscv, left, right superior caval vein; lv, left ventricle; oft: outflow tract; pv, pulmonary vein; r, l-pr: right, left pulmonary ridge; rsh, lsh, right, left sinus horn; rv: right ventricle; sp, septum primum; v, primitive ventricle; vv, venous valves. Scale bar: *A–C* = 100 μm; *D* = 100 μm, *E* = 10 μm.

Antibody staining confirmed heterogeneous Ankrd1 protein expression in developing cardiomyocytes (*Figure 1D*). Subcellular protein localization was always detected at the sarcomeric I band (*Figure 1E*); additional nuclear localization was frequently observed in E10.5 cardiomyocytes (*Figure 1Ea, b*) but was no more detectable by E14.5 (*Figure 1Ec, d*).

3.2 ANKRD1 finely modulates rotation and remodelling in the early myocardium

We next aimed to assess the effects of a genetically-based increase in ANKRD1 levels on cardiac structure and functionality. Thus, we generated two transgenic (Tg) mouse lines overexpressing human ANKRD1

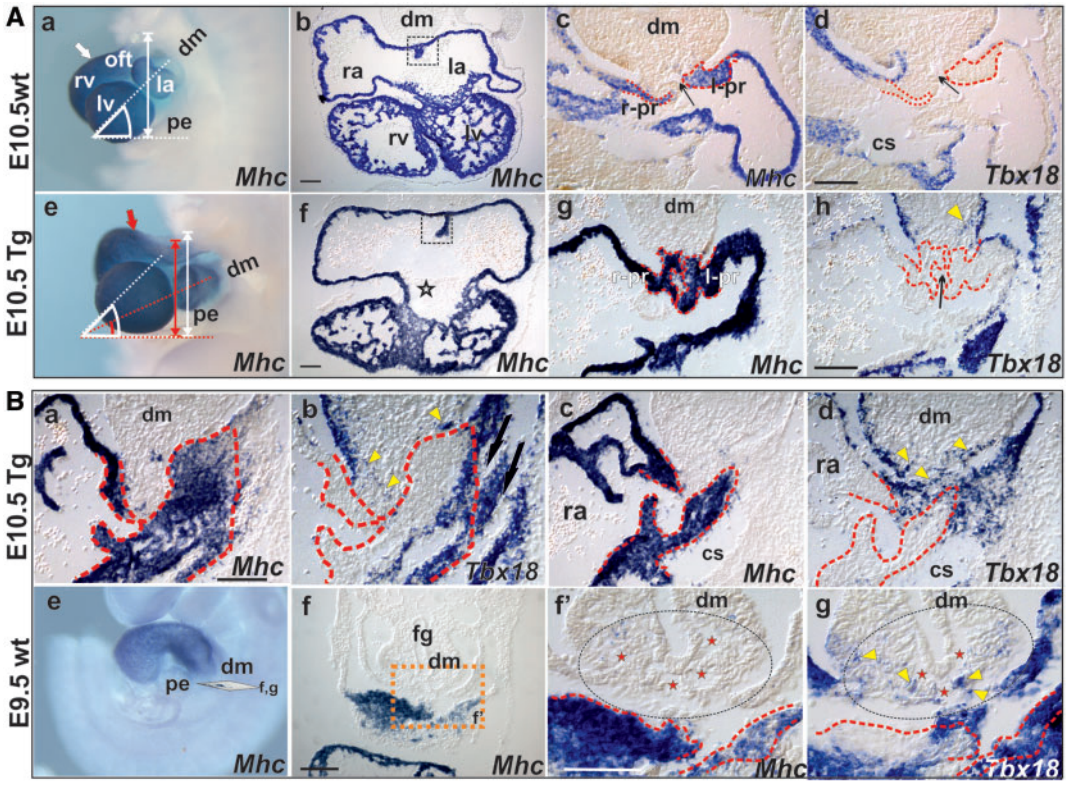

Figure 2 ANKRD1 overexpression affects fine rotation and remodelling in the early myocardium. (*A*) Abnormal rotation and remodelling in E10.5 Tg compared to wt embryos, ISH whole mount (*a*, e) and on sections (*b–d*, *f–h*) analysis. Dotted lines in *a*, e show LA-LV angle in wt (white) and Tg (red); double-headed arrow shows cranio-caudal extension of the heart from the LV base to the outflow tract. (*b*, *f*) Abnormal shape and position of cardiac chambers, atrioventricular canal (asterisk), and septum primum (dotted box) in Tg. Red dotted lines in *c*, *d*, *g*, *h* indicate the myocardium of the pulmonary ridges. Black arrow indicates the pulmonary pit, misplaced in Tg embryos. Yellow arrowheads indicate Tbx18^{+} cells within the dorsal mesocardium (dm). (*B*) Venous pole organization in E10.5 Tg (*a–d*) and E9.5 wt (e–g) embryos, ISH on sections (*a–d*, *f*, *g*), and whole mount (e). Red dotted lines delineate the sino-atrial myocardium. Yellow arrowheads indicate *Tbx18*$^{+}$ cells within the dm. Black dotted circle in *f'*, *g* highlights the base of the dm where some Tbx18^{+} cells are visible, flanking the loosely arranged mesoderm (red asterisks). fg, foregut; pe, proepicardium. See *Figure 1* legend for other abbreviations. Scale bar: *A*, *B* = 100 μm.

in the myocardium under *Myh6* gene promoter (Supplementary material online, *Figure S1A*), which is active from E7.5 onwards.[27] Transgene protein levels were very modest in E10.5 and E14.5 embryos (Supplementary material online, *Figure S1A* and *B* and not shown), but increased, to a similar order of magnitude, in neonatal and 10M Tg hearts (Supplementary material online, *Figure S1A*). ANKRD1 transgene presented always a sarcomeric sub-localization, however, some nuclear signal was additionally visible in adult Tg hearts (Supplementary material online, *Figure S1C*). Preliminary analysis did not reveal phenotypic differences between the two Tg lines (not shown), thus detailed analysis was performed on a single line.

We initially investigated early cardiac development. E10.5 Tg hearts presented well-developed atrial and ventricular chambers, which however appeared more compressed along the cranio-caudal and dorso-ventral axes, were laterally displaced and presented a reduced rotational angle if compared to wt littermates (*Figure 2Aa*, e). In particular, the sino-atrial region was more caudally oriented in Tg hearts, similarly to E9.5 wt embryos (*Figure 2Be*). Compressed shape and malrotation affected both internal remodelling and the relative orientation between sino-atrial myocardium, the flanking dorsal mesocardium, and the proepicardium (*Figure 2Aa*, e). This resulted in malpositioning of the developing septum primum, of the pulmonary ridges, as well as of the sinus horns myocardium, visualized by Tbx18 expression[28] (*Figure 2Ac*, *d*, *g*, *h*). The sinus horns confluence, which defines the entrance of the cardinal veins into the sino-atrial region, and the pulmonary pit, delineating the route of canalization of the PV, were distinct in Tg hearts as in wt embryos. However, in Tg hearts, a mesh of Tbx18^{+} mesenchyme was additionally detected within the dorsal mesocardium. Tbx18^{+} mesenchyme was more abundant caudally, in proximity of the differentiating sinus horns myocardium (*Figure 2Ba–d*) and extended cranially up to the pulmonary ridges (*Figure 2Ag*, *h*). Remarkably, a corresponding situation could be detected in E9.5 wt embryos, which presented some Tbx18^{+} cells within the loosely arranged dorsal mesocardium at the proepicardial border (*Figure 2Bf*, *g*).

In conclusion, E10.5 Tg hearts, although apparently progressed in development, are 'cast' into a more immature topological arrangement that strongly affects venous pole remodelling.

3.3 ANKRD1 Tg hearts present SV defects

By mid-foetal stages, most Tg hearts presented a misshapen sino-atrial region. Three-dimensional anatomically-based reconstruction outlined

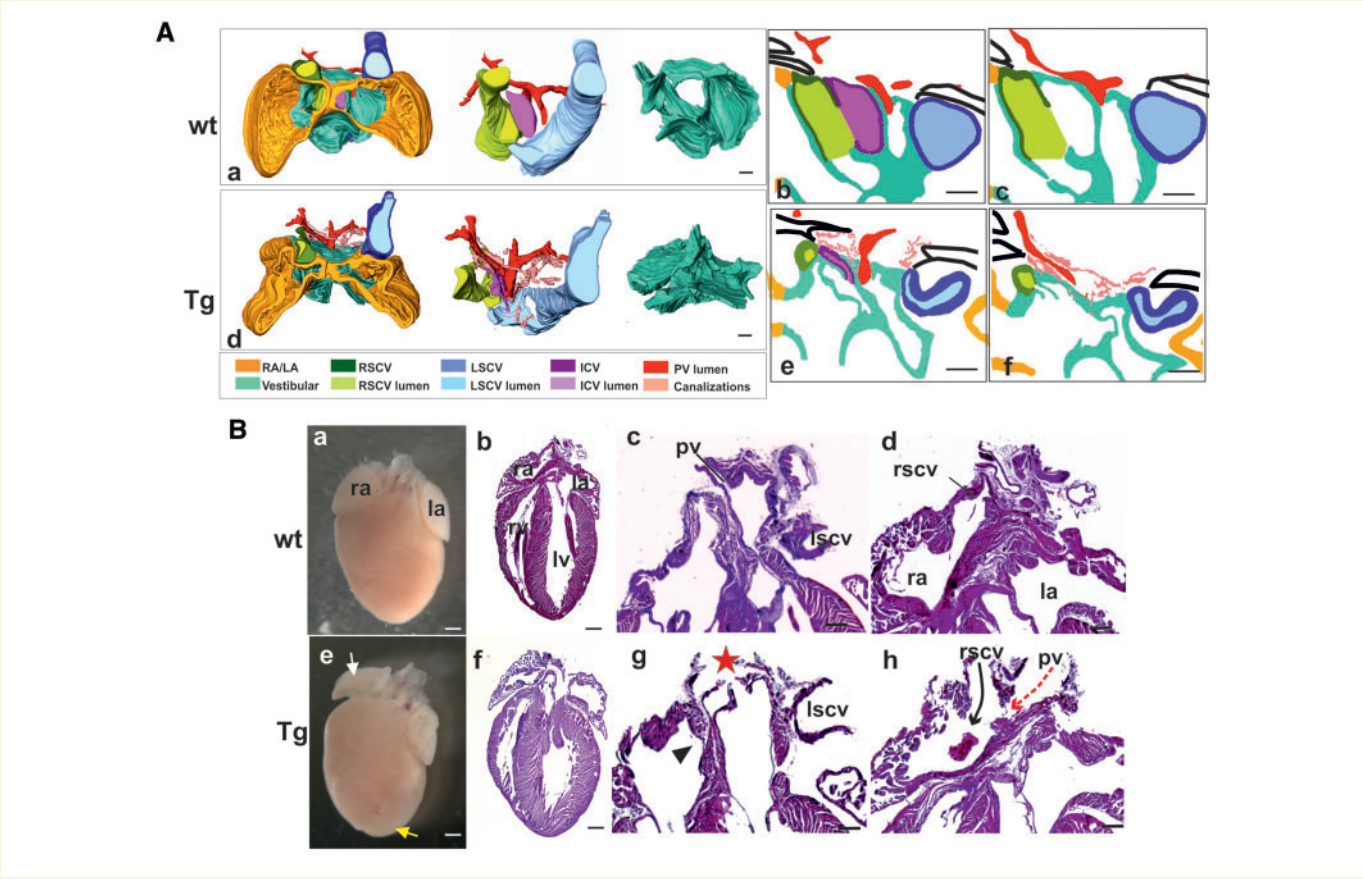

Figure 3 SV defects in mid-foetal and neonatal ANKRD1 Tg hearts. (*A*) Three-dimensional reconstruction of the sino-atrial region and venous system lumen in E13.5 hearts, highlighting anomalous venous pole organization in Tg hearts. Note in *d*, the canalizations around PV and systemic veins and *a* compressed shape of the vestibular region; (*b*, *c*, e, *f*) virtual sections at the venous pole. In Tg embryos, the communications between PV and systemic veins around the vestibular regions define the SV defects. Black lines delineate splanchnopleure. (*B*) Neonatal hearts, freshly isolated (*a*, e), and H/E analysis (*b–d*, *f–h*). (*c*) White arrow indicates atrial malrotation, yellow arrow indicates rounded ventricular apex. (*g*, *h*) SV defects in Tg hearts. Confluence of RSCV and PV at the dorsal atrial wall (asterisk in *g*) and into the RA (*h*) are clearly recognizable. Black arrowhead in *g* indicates the misshapen fossa ovalis. See *Figure 1* legend for abbreviations. Scale bar: *Aa–f* = 100 μm; *Ba*, *b*, e, *f* = 500 μm; *Bc*, *d*, *g*, *h* = 200 μm.

the malpositioning of venous inlets, which however drained in the correct atrial chamber (*Figure 3A*). Additionally, Tg hearts presented a network of microcanalizations, delineating a fine network of ectopic connections between the PV and systemic veins, which partially drained into the vestibular region through small fenestrations (*Figure 3Ad, f* and Supplementary material online, *Figure S3*). These anomalous veno-atrial connections have been associated to SV defects in humans.[29] Anomalous veno-atrial connections were normally accompanied (20/27 embryos) by atrioventricular rotational defects and compressed appearance of the vestibular region (*Figure 3Ad* and Supplementary material online, *Figure S3*). However, in a minority of Tg embryos (7/27) SV defects occurred in the absence of morphogenetic impairment (not shown), thus indicating higher venous pole sensitivity to increased *ANKRD1* expression.

At the early postnatal life, only subtle differences could be detected between wt and Tg hearts by external anatomical observation (*Figure 3Ba,* e), however, SV defects could be clearly outlined histologically (*Figure 3Bb–d, f–h*). A misshapen fossa ovalis was also clearly recognizable (*Figure 3Bg*).

In conclusion, ANKRD1 Tg hearts present SV defects. Fine alterations in cardiac venous pole remodelling impact both systemic and PV development, which are closely interwined.[30] Our data support the hypothesis that SV defects are likely originated by impaired remodelling of the sino-atrial myocardium during embryonic development.

To investigate the mechanisms for SV defects, we initially wondered whether master transcription factors *GATA4* and *Nkx2.5*, functionally associated to ANKRD1, could be transcriptionally affected in early Tg embryos. qPCR analysis showed that *GATA4* and *Nkx2.5* mRNA levels were increased in E10.5 Tg hearts ($P < 0.05$ for *Nkx2.5*), however, this difference was blunted at E14.5 (*Figure 4A*). These results indicate that very low ANKRD1 overexpression is sufficient to affect *GATA4* and *Nkx2.5* transcription, however, exclusively within the short time window of ANKRD1 nuclear localization. Thus, *GATA4-Nkx2.5* transcriptional modulation could be involved in SV defects onset.

As cardiac remodelling occurs thought the entire foetal period, these results raise the possibility that additional ANKRD1-mediated mechanisms should account for phenotype progression in Tg hearts, including altered chamber morphology. ISH analysis of E14.5 Tg hearts did not show differences in regional distribution of genes which delineate and/or define myocardial landmarks and compartments, such as *Pitx2* (left–right identity),[31] *Tbx3* (primary myocardium),[32] *Nppa*, *Gja5* (chamber myocardium),[32,33] *Mlc2v* (ventricular myocardium),[33] *Bmp10* (trabecular

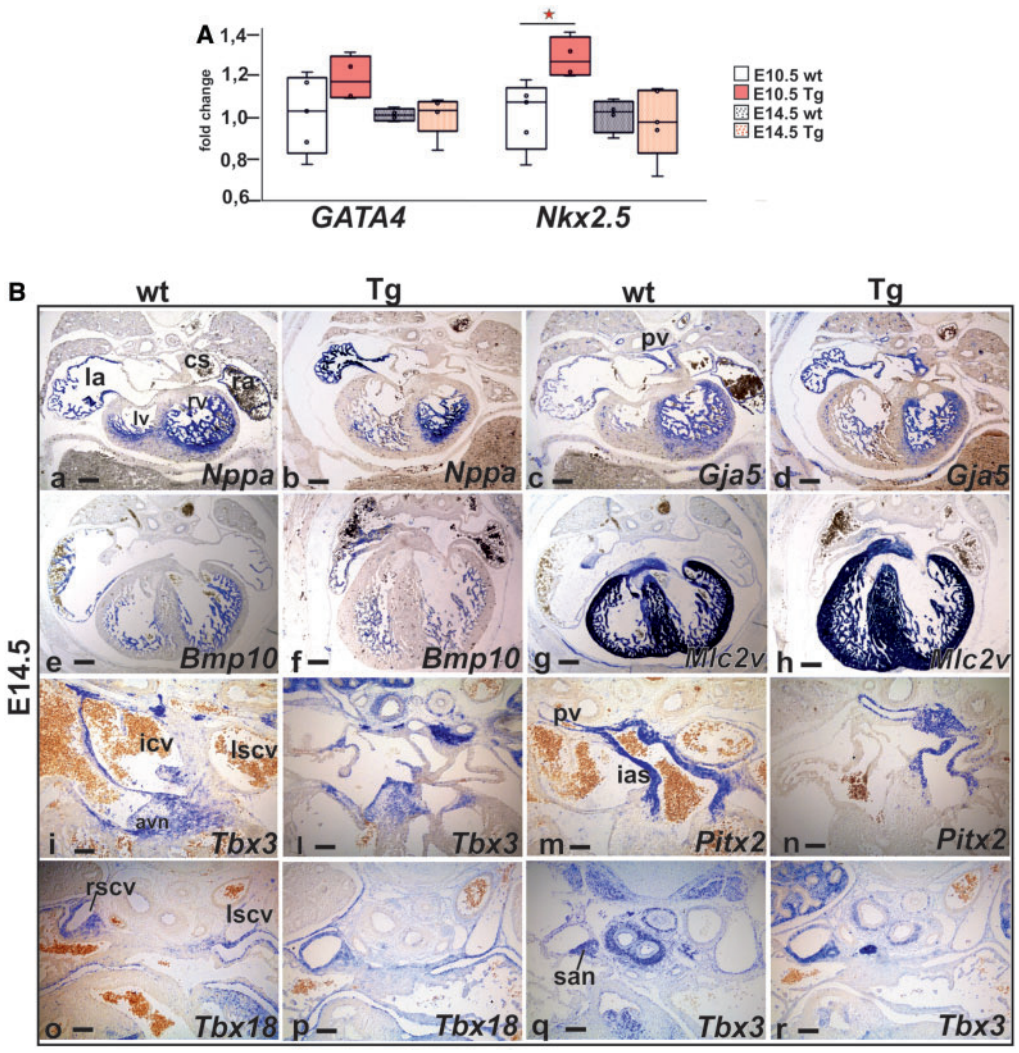

Figure 4 Timed transcriptional modulation in ANKRD1 Tg embryos. (*A*) *GATA4* and *Nkx2.5* mRNA expression levels in E10.5 (wt = 5, Tg = 4) and E14.5 (wt = 4, Tg = 5) hearts, $*P < 0.05$, Student unpaired *t*-test; values are compared to the mean wt level at each stage. (*B*) ISH analysis shows that molecular patterning is not affected in E14.5 Tg hearts. avn, atrio-ventricular node; icv: inferior caval vein; san, sino-atrial node; for other abbreviations, see *Figure 1* legend. Scale bar: *a–h*: 20 μm; *i–r*: 10 μm.

myocardium),[34] and *Tbx18* (SH myocardium)[28] (*Figure 4B*), thus ruling out late transcriptional effects on myocardial patterning.

3.4 Adult ANKRD1 Tg mice develop progressive ventricular diastolic dysfunction

We next investigated the consequences of ANKRD1 overexpression in adult life. Tg mice were born according to Mendelian ratio, however by 10 months (10M) they presented a reduced viability (88, 5%Tg vs. 96, 9%wt; $P < 0.05$). Histological analysis uncovered a severely dilated left atrium in all Tg hearts (*Figure 5A*). LA thrombi, patent foramen ovale (PFO), ventricular dilatation, and altered chamber geometry could additionally be detected as isolated or combined defects (*Figure 5A*). Moderate fibrosis was detected in ventricular (*Figure 5Am, n*), but not atrial chambers, except for the organized thrombi (*Figure 5Ag, h*). Accordingly, TGFβ levels and TGFβ- activated ERK1/2 phosphorylation[35] were moderately increased in Tg hearts (Supplementary material online, *Figure S4*).

We compared wt and Tg cardiac function by echocardiography and haemodynamic analysis at 2M and 10M (*Table 1*). Echocardiography indicated preserved LV systolic function (i.e. EF and FS values) in 2 and 10M Tg mice, and absence of ventricular hypertrophy at 10M. However, transmitralic flow analysis in 2M mice revealed comparable *E/A* ratio but higher DT values in Tg animals, suggesting an initial diastolic dysfunction. By 10M, remarkably increased E/A ratio and reduced DT value were found in Tg mice, indicating progression of diastolic dysfunction with aging. Remarkably increased MPI[36] in 10M Tg vs. wt mice supports this notion.

PV flow analysis revealed the presence of a small late diastolic wave (*d2*) in 2M Tg mice (6/8) (*Figure 5B*), indicating additional blood inflow into the left atrium, presumably via the identified cavo-pulmonary shunts

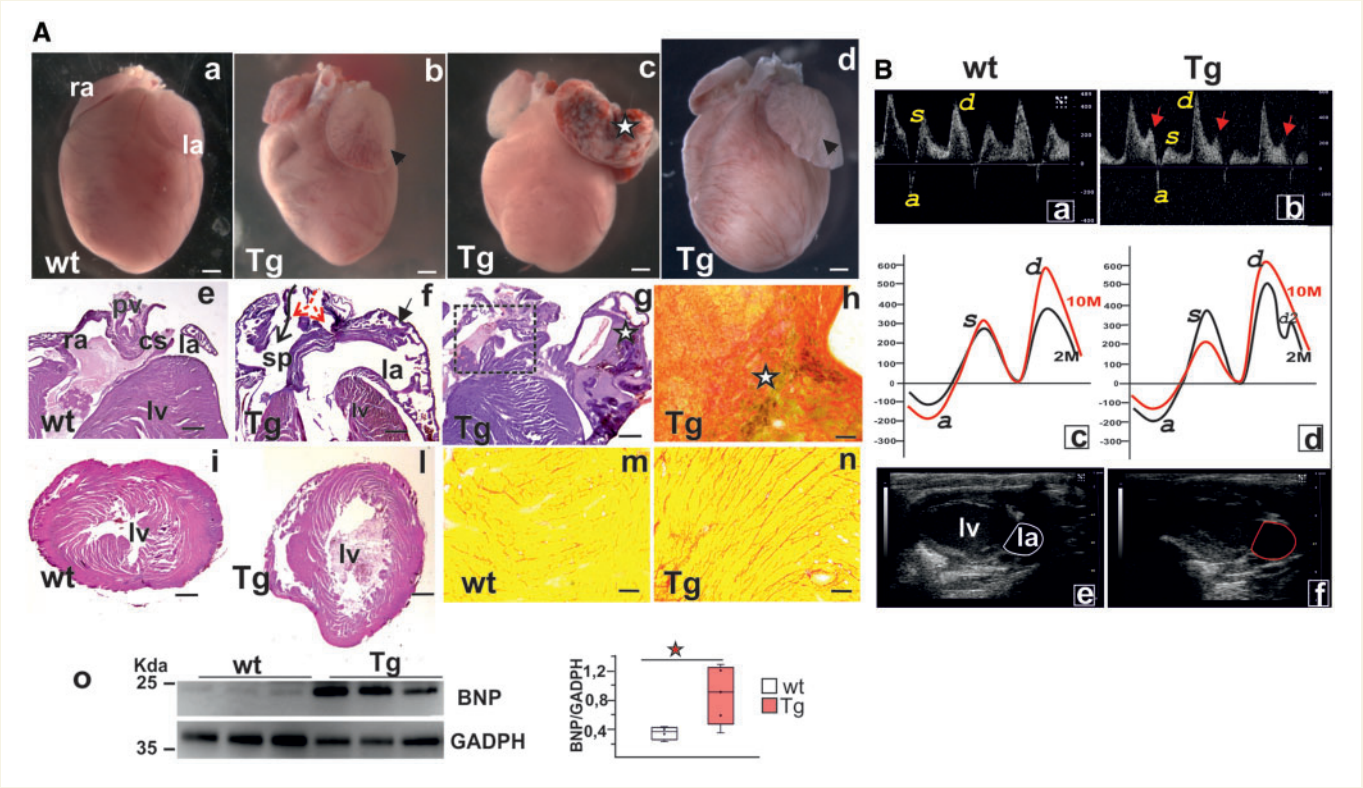

Figure 5 Adult ANKRD1 Tg hearts analysis. (*A*) Phenotypic variability in 10M Tg hearts. (*a–d*) Freshly isolated hearts; (e–*n*) histological analysis, sino-atrial (e–*h*), and ventricular (*i–n*) regions; H/E (e–*g*, *i–l*) and Sirius red (*h*, *m*, *n*) staining. Black arrowhead indicates the enlarged Tg LA, asterisk indicates thrombus. (e–*h*) Note in (*f*) anomalous confluence of PV (red dotted arrow) and RSCV (black arrow) at the dorsal atrial wall. (*g*) Dotted box indicates PFO, associated to thrombus formation. (*h*) Fibrotic infiltration within LA thrombus. (*i–l*) Dilatation and altered geometry in Tg LV; (*m*, *n*) moderate fibrosis in Tg LV. (*o*) Western blot analysis of BNP vs. GADPH expression in 10M wt ($n = 4$) and Tg ($n = 5$) hearts, representative results and box plot quantification; $^*P < 0.05$, Student unpaired *t*-test. Scale bar: *a–d* = 1 mm, e–*g*, *i–l* = 0.5 mm, *g–i* = 100 µm. B: *In vivo* analysis. (*a*, *b*) PV Doppler flow profile of a representative 2M wt (*a*) and Tg (*b*) mouse. Red arrows indicate *d2* wave in Tg. (*c*, *d*) Representation of mean PV Doppler flow curves in wt and Tg mice at 2 and 10M. Mean *a*, s, and *d* values are from *Table 1*. (e, *f*) Echocardiographic view of a 10M wt (e) and Tg (*f*) heart. Note strongly enlarged LA in Tg (red line).

(*Figure 3B* and *Figure 5A*). We hypothesize that cavo-pulmonary shunts became haemodynamically significant only in late diastole due to onset of a temporary pressure gradient which favours the R to L shunt. The *d2* wave was no longer detected in 10M Tg, indicating a change in L/R atrial chamber pressure gradients with age.

At 2M, *a* wave value was significantly higher in Tg than wt mice, indicating more effective atrial contraction (*Table 1* and *Figure 5B*). s and *d* wave values were also higher in Tg than wt mice (*Table 1* and *Figure 5B*), indicating ventricular systolic compensation according to Frank Starling law. Comparable *a/d* ratio indicated similar haemodynamics in 2M wt vs. Tg mice during atrial systole and ventricular diastole; however, *s/d* ratio was <1 in 2M Tg mice, as it occurs in early diastolic dysfunction.[37] By 10M, decreased *a* and s values, as well as *s/d* and *a/d* ratio indicated less effective atrial contraction and very different haemodynamics in Tg vs. wt mice, underlying a severe diastolic dysfunction and loss in LA contractility. Doppler visualization confirmed this latter finding. Visual assessment of mitral valve flow did not reveal anomalies in valve functionality, thus ruling out valvular impairment as the leading cause for diastolic dysfunction.

Overall, functional analysis indicates that 2M Tg mice present initial ventricular diastolic dysfunction accompanied by increased atrial contractility; by 10M, diastolic dysfunction progresses into diastolic HF, associated to LA enlargement and loss of LA contractility. In line, cardiac disease marker BNP was also significantly increased in 10M Tg hearts (*Figure 5Ao*).

Atrial dilatation and diastolic HF together can lead to pulmonary oedema, whereas diastolic HF can occasionally lead to ventricular fibrillation. Thrombi formation in 10M Tg mice indicates altered atrial haemodynamics, possibly caused by HF and/or PFO defects.[38] All these comorbidities can have a fatal outcome, therefore they likely account, as single or combined events, for the reduced viability in 10M Tg mice.

3.5 Cardiomyocyte contractility is impaired in ANKRD1 Tg hearts

We tested the hypothesis that impaired cardiomyocyte contractility could contribute to CHD and adult diastolic dysfunction in Tg hearts. Isolated myofibrils from mid-foetal, early postnatal, and 10M hearts were tested for passive tension. Neonatal and 10M myofibrils were additionally tested for active mechanical properties.

Sarcomere length-resting tension (SL-RT) relations (i.e. passive mechanical properties) of wt and Tg myofibrils were comparable at E14.5

Table 1 Ecocardiographic (top) and haemodynamic (botton) analysis of wt and ANKRD1 Tg mice at 2 and 10 months; *n* = number of animal analysed (2M: wt = 6 males, 4 females; Tg = 3 males, 5 females; 10M: wt = 6 males, 3 females, Tg = 2 males, 5 females)

	Wt 2M (*n* = 10)	Tg 2M (*n* = 8)	Wt 10M (*n* = 9)	Tg 10M (*n* = 7)	Wt vs. *Tg* @2M (*P*)	Wt vs. Tg @10M (*P*)	Wt: 2M vs. 10M (*P*)	Tg: 2M vs. 10M (*P*)
LV%EF	56.80 ± 3.64	63.75 ± 4.87	58.25 ± 2.94	63.29 ± 4.03	0.23	0.22	0.87	1
LV%FS	29.40 ± 2.53	34.50 ± 3.39	30.25 ± 1.91	34.43 ± 2.90	0.25	0.20	0.93	1
IVSd	–	–	1.05 ± 0.05	0.96 ± 0.07	–	0.31		–
IVSs	–	–	1.48 ± 0.03	1.43 ± 0.05	–	0.56	–	–
LVIDd	–	–	3.89 ± 0.14	3.81 ± 0.15	–	1	–	–
LVIDs	–	–	2.69 ± 0.15	2.50 ± 0.19	–	0.30	–	–
LVPWd	–	–	0.97 ± 0.04	0.94 ± 0.06	–	0.90	–	–
LVPWs	–	–	1.36 ± 0.04	1.15 ± 0.10	–	0.05*	–	
E/A	2.13 ± 0.21	2.04 ± 0.27	2.06 ± 0.23	3.13 ± 0.57	0.95	0.10	1	0.06
DT	19.05 ± 2.12	23.01 ± 3.12	14.90 ± 1.66	14.26 ± 2.14	0.41	0.79	0.23	0.06
MPI	0.79 ± 0.04	0.80 ± 0.07	0.71 ± 0.04	0.86 ± 0.06	0.89	0.06	0.55	0.45
d	363.20 ± 63.65	507.25 ± 75.27	587.13 ± 121.23	629.43 ± 132.17	0.14	0.86	0.91	0.19
d2	np	298.5 ± 39.90	np	np	–	–	–	–
a	-111.40 ± 13.18	-187.63 ± 30.36	-191.13 ± 71.75	-132.57 ± 37.56	0.03*	0.86	0.91	0.12
s	271.20 ± 13.18	371.88 ± 30.36	311.00 ± 71.75	203.86 ± 37.56	0.17	0.02*	0.41	0.03*
s/d	1.01 ± 0.22	0.66 ± 0.08	0.80 ± 0.22	0.34 ± 0.04	0.45	0.01*	1	0.02*
a/d	-0.37 ± 0.05	-0.40 ± 0.07	-0.30 ± 0.06	-0.21 ± 0.03	0.82	0.22	1	0.08
a/s	-0.45 ± 0.08	-0.60 ± 0.08	-0.49 ± 0.12	-0.62 ± 0.08	0.12	0.32	0.32	0.67

Values are indicated as mean ± SE. *$P \leq 0.05$.
LV% EF, LV ejection fraction; LV%FS, LV fractional shortening; IVSd, interventricular septum diastolic thickness; IVSs, interventricular septum systolic thickness; LVIDd, LV internal diameter, diastolic; LVIDs, LV internal diameter, systolic; LVPWd, LV posterior wall, diastolic; LVPWs, LV posterior wall, systolic; MPI, myocardial performance index; *np*, not present. See text and Supplementary material online, *Methods* for other abbreviations. Wt vs. Tg data comparison at each stage (2M, 10M) was performed by Mann–Wilcoxon W test; 2M vs. 10M data comparison for each experimental group (wt and Tg) was performed by Wilcoxon signed-rank test.

(*Figure 6Aa*) and 10M (*Figure 6Ac*), but not in newborns (*Figure 6Ab*). Interestingly, neonatal wt myofibrils retained passive properties of foetal stage, as expected,[39] whereas Tg myofibrils presented a functional shift towards the stiffer phenotype of adult wt (*Figure 6Ab, c*).

Regarding active mechanical properties (*Figure 6Ad*), the maximally calcium activated isometric force value (P_0) was significantly higher in neonatal Tg than wt myofibrils, and comparable to adult wt value. Kinetics of force rise (k_{ACT}) and relaxation (slow and fast k_{REL}) and tension relaxation parameters (D_{slow}) were comparable in neonatal Tg and wt myofibrils. Interestingly, adult wt and Tg myofibrils showed comparable k_{ACT}, while force relaxation was clearly impaired in Tg, as shown by significantly increased D_{slow} and decreased fast k_{REL}. Thus, Tg myofibrils present a differential modulation of passive and active contractile properties during life time, i.e. reduced compliance at neonatal stage and overall slowed down relaxation at 10M.

We investigated the molecular basis for early functional changes observed in Tg myofibrils. Regulation of passive mechanical properties is mainly due to modulation of titin compliance either post-transcriptionally, or at the transcriptional level via alternative splicing.[40,41] Here, we tested the hypothesis that titin transcription could be affected in ANKRD1 Tg hearts. Titin splicing regulation involves N2B/N2BA isoforms ratio modulation and N2BA length modification via exons inclusion at the middle Ig and PEVK spring regions.[40,41]

In E14.5 Tg hearts, the transcripts levels of titin did not show significant differences, similar to representative thick, thin and Z band components (*Figure 6B*). The N2B/N2BA isoform ratio was slightly, though not significantly, increased (*Figure 6C*). In neonatal Tg hearts, expression of analysed transcripts were unchanged (*Figure 6B*). However, N2B/N2BA ratio was now clearly modified and significantly reduced in Tg samples (*Figure 6C*), indicating a transcriptional shift towards the more compliant N2BA isoform. This result was somehow surprising, since functional data indicated a reduced compliance in neonatal Tg myofibrils (*Figure 6Ab*). Intriguingly, when we performed PCR scanning analysis of N2BA exon usage within middle Ig and PEVK regions, we found that Tg hearts used a different exon combination, leading to expression of shorter, therefore less compliant, N2BA titin isoforms (*Figure 6C* and Supplementary material online, *Figure S5*). Thus, a wide modulation within titin gene transcription accompanies the biomechanical changes of neonatal Tg myofibrils.

3.6 Cardiomyocyte organization and ultrastructure are progressively impaired in ANKRD1 Tg mice

Having established that ANKRD1 overexpression impairs sarcomeric function, we next explored the impact of these alterations on cellular organization. Cardiomyocyte disorganization was visible in Tg hearts from E10.5 onwards (*Figure 7A*). Confocal analysis showed that E14.5 Tg cardiomyocytes were mostly distorted and presented sarcomeric disaligment (*Figure 7Ai, l*, Supplementary material online, *Videos S1* and *S2*). Electron microscopy analysis of neonatal Tg ventricles confirmed sarcomeric disorganization and additionally showed focal areas of myofibrillar disruption (*Figure 7Bf, i*). Swollen mitochondria with abnormal cristae (*Figure 7Bi*) and rare lipid droplets in the cytoplasm (*Figure 7Bf*) were also found. By 10M, ultrastructural disorganization progressed in Tg ventricles, as indicated by the increased myofibril loss, mitochondrial damage

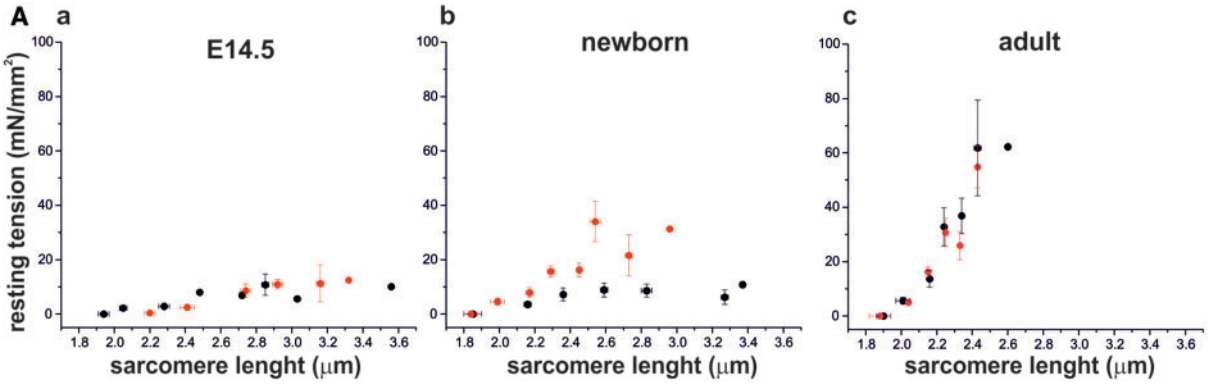

d

Myofibril batch	SL μm	Active tension P_0 mN mm^{-2}	Active tension k_{ACT} s^{-1}	Tension relaxation D_{slow} ms	Tension relaxation Slow k_{REL} s^{-1}	Tension relaxation Fast k_{REL} s^{-1}
Newborn						
WT (8)	2.26±0.04	72±4.5	6.07±0.40	93±7	1.64±0.27	14±1.2
TG (5)	2.21±0.03	136±19*	5.43±0.45	99±6	1.92±0.36	14±1.2
Adult						
WT (6)	2.12±0.03	141±14	7.27±0.47	71±5	3.27±0.26	41±6
TG (5)	2.14±0.05	182±21	6.14±1.5	96±6#	2.96±0.91	18±5#

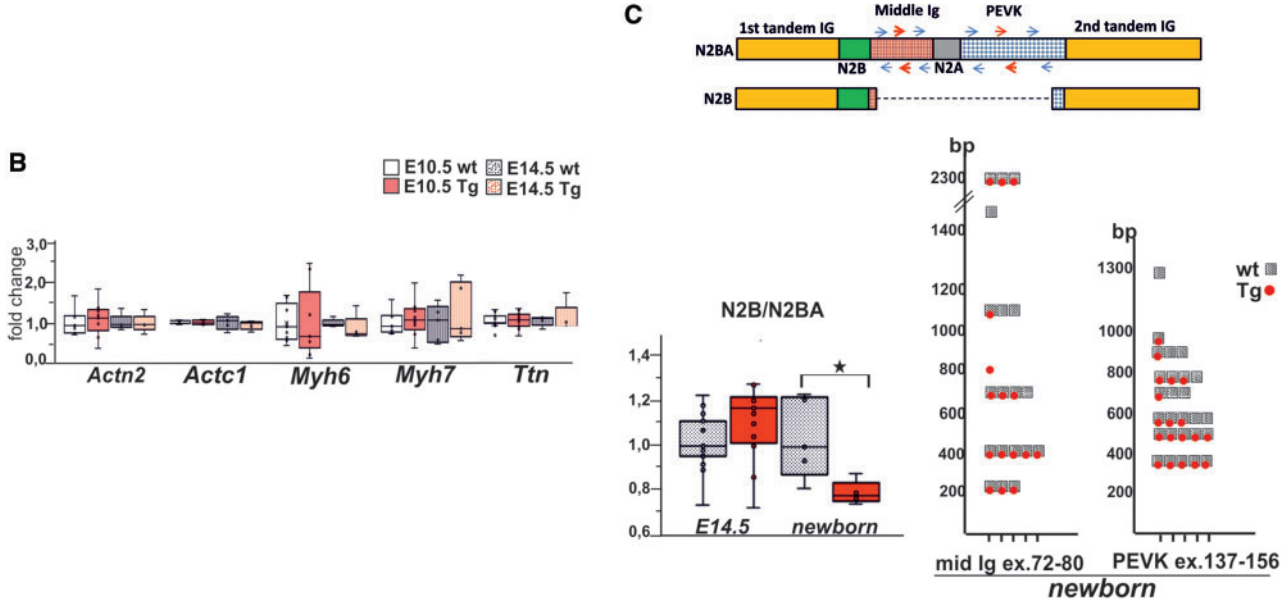

Figure 6 Modulation of contractile properties in ANKRD1 Tg hearts. A: functional analysis on isolated myofibrils. (*a–c*) Average sarcomere length-resting tension relation of myofibrils from E14.5 (*a*) newborn (*b*) and adult (*c*) hearts; wt, *black circle*; Tg, *red circle*. Vertical and horizontal bars are SEM. (*d*) Mechanical properties of myofibrils from newborn and adult hearts (myofibrils number in brackets). D_{slow}, duration of the slow linear phase of relaxation; k_{ACT}, rate constant of force development following maximal Ca^{2+}-activation; P_0, maximum isometric tension; SL, sarcomere length; Slow-Fast k_{REL}, rate constants of tension relaxation for slow and fast relaxation phases. *P < 0.001, #P < 0.02, Student unpaired *t*-test. (*B*) qPCR results of sarcomeric genes expression in E14.5 and newborn hearts. wt vs. Tg: $P > 0.05$ for each stage, Student unpaired *t*-test; values are compared to the mean wt level at each stage. (*C*) Titin splice variant analysis. Top: schematic representation of titin N2BA and N2B structure; arrows indicate position of primers used for N2BA combinatorial exon analysis, red arrows: regions with differential exon inclusion in newborn wt/Tg. Bottom left: N2B/N2BA isoform ratio analysis. *$P < 0.05$, Student unpaired *t*-test; values are compared to the mean wt level at each stage. Bottom right: PCR amplification of exons 72–80 and exons 137–156 from wt and Tg hearts ($n = 5$) results in multiple amplicons (square boxes) of different length. The longest amplicons are mostly detected in wt hearts. *Y*-axis: amplicons length (bp); *X*-axis: count of wt and Tg samples which present the specified amplicon (see Supplementary material online, *Figure S5* for original data).

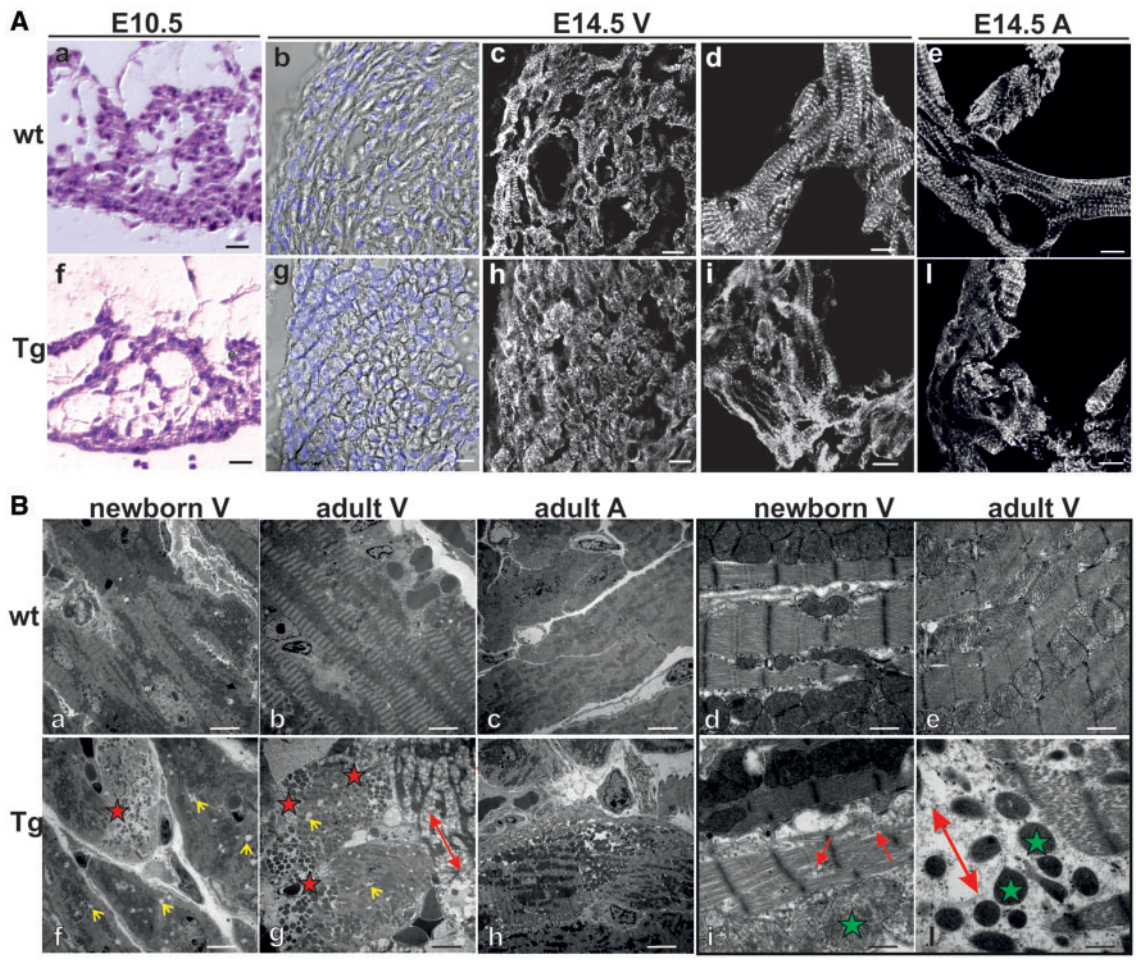

Figure 7 Impairment of cardiomyocyte organization and ultrastructure in ANKRD1 Tg hearts. (*A*) Cardiomyocyte organization in embryonic wt and Tg hearts. H/E analysis at E10.5 (*a*, *f*) and confocal analysis of E14.5 RV wall (*b*, *c*, *g*, *h*), trabeculae (*d*, *i*), and atria (e, *l*); (*b*, *g*) bright field and nuclei, merged; (*c*–e, *h*–*l*) actinin. *b*, *c* and *g*, *h* are adjacent sections. Scale bar: *a*, *f* = 20 μm; *b*–e, *g*–*l* = 10 μm. (*B*) TEM analysis of neonatal and adult ventricles and of adult atria, at low (*a*–*c*, *f*–*h*) and high magnification (*d*, e, *i*, *l*). Red asterisk, focal sarcomeric loss; red arrow, sarcomeric disorganization; double headed arrow, extensive sarcomeric loss; green asterisk, damaged mitocondria; yellow arrowheads, lipid droplets. Scale bar: *a*–*c*, *f*, *h* = 5 μm; *d*, e, *i*, *l* = 1 μm.

and accumulation of lipid droplets. Myofibrillar loss was not detected in adult Tg LA (*Figure 7*).

In conclusion, tight regulation of *ANKRD1* expression is required for proper modulation of cardiomyocyte structure and of sarcomeric assembly and stability, from early development to adult life. Impaired embryonic remodelling and contractility in ANKRD1 Tg mice are therefore underlined by a common cellular basis.

4. Discussion

Here, we have presented the first longitudinal study aiming to assess the consequences of ANKRD1 myocardial overexpression from development to adult stage. Novel findings of our study are: (i) the presence of SV defects in ANKRD1 Tg mice. To our knowledge, this is the first mouse model for such CHD. (ii) The pathological phenotype of adult ANKRD1 Tg hearts in the absence of pharmacological stimuli or pressure overload. This feature has not been highlighted before,[16] possibly because of late appearance of gross cardiac abnormalities. The mechanistic link between ANKRD1 overexpression, CHD and adult cardiomyopathy are hereafter discussed, in relation to ANKRD1 expression and subcellular localization.

4.1 ANKRD1 expression and overexpression

We have here shown a discrete sub-compartmentalization of *Ankrd1* expression and dynamic nucleo-sarcomeric localization in the developing heart, not recognized in previous studies.[5,7] The limited time window of nuclear localization suggests that ANKRD1 can sense ongoing haemodynamic changes[42] and respond by fine tuning its interacting partners (*Figure 8A*).

Extreme sensitivity to increased ANKRD1 levels in Tg hearts is therefore not surprising. Very low levels of Tg expression in E10.5 Tg hearts were sufficient for morphological and cellular phenotype onset and for

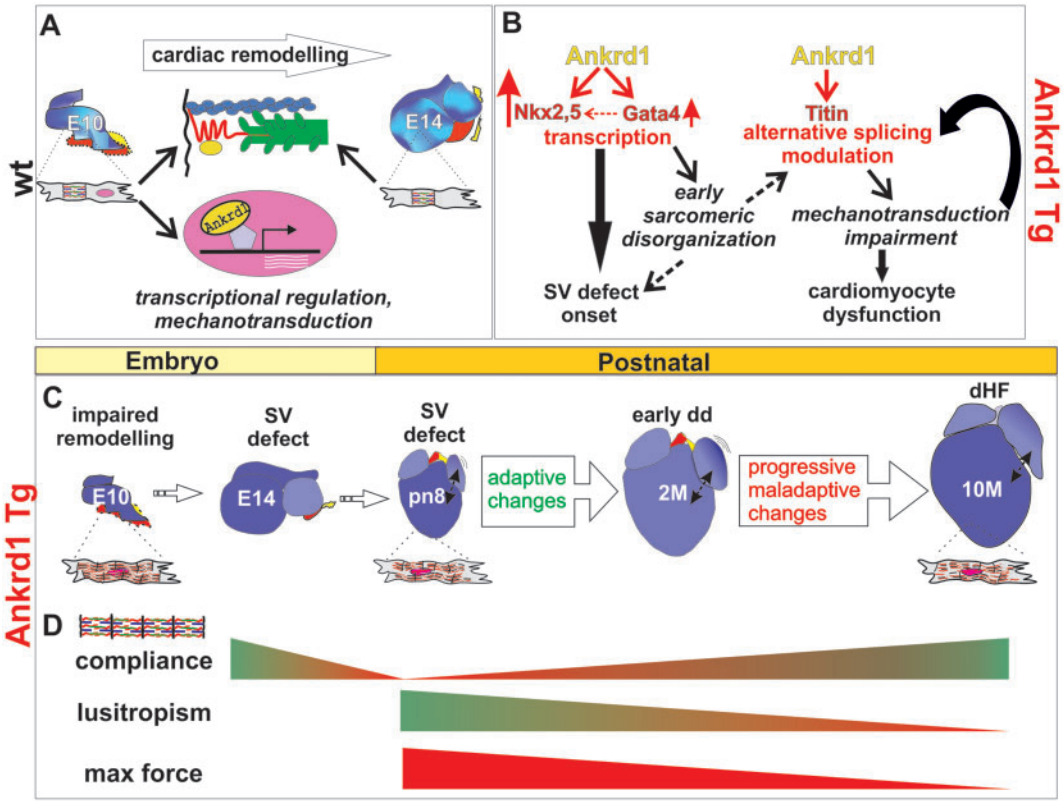

Figure 8 Working model linking ANKRD1 expression, overexpression and cardiac disease. (*A*) Ankrd1 role in heart development. Heterogeneous Ankrd1 expression and its dynamic nucleo-sarcomeric sub-localization modulate developmental cardiac remodelling in response to haemodynamics by finely regulating cardiomyocyte transcription and mechanotransduction; the initially contiguous PV (yellow, dotted lines) and systemic veins (red, dotted lines) precursors become spatially separated by mid-fetal stage. (*B*) Temporally distinct transcriptional modulation scored in embryonic and neonatal Tg hearts (red arrows) and their proposed link with disease onset and early progression at the cellular and organ levels (black arrows). (*C* and *D*) Disease onset and progression in Tg hearts, with the underlying cardiomyocyte defects (*C*) and myofibrillar functional modifications (*D*). Embryos: impaired myocardial remodelling retains the contiguity of the regions where PV and systemic veins precursors are located, thereby causing SV defect. Postnatal life: neonatal Tg hearts present overt cardiomyocyte structural and functional impairment. Altered A-V haemodynamic cross talk (double headed arrow), due to SV defect and impaired functionality in Tg cardiomyocytes, initiates a vicious loop that progressively leads to diastolic dysfunction (dd), then heart failure (dHF). (*D*) Tg myofibrillar functional properties (compliance, lusitropism and maximal force) present substantial modifications in prenatal and postnatal life, as shown by reduced and then increased compliance, progressive reduction of lusitropism, and persistent higher maximal force. Colour code: green, values in Tg myofibrils comparable to corresponding wt; red: values higher than wt.

transient *GATA4* and *Nkx2.5* transcriptional up-regulation. ANKRD1 expression can in turn be regulated by Nkx2.5 and GATA4[5,6,9] Thus, our data suggest a novel *in vivo* autoregulatory loop for increased *GATA4* and *Nkx2.5* transcription, mediated by ANKRD1 binding. We cannot rule out that GATA4 could be directly involved in *Nkx2.5* transcriptional activation.[43] GATA4-ANKRD1 functional interaction can lead to increased GATA4-mediated sarcomeric gene expression and has been proposed to contribute to sarcomere homeostasis.[9,10] On the other hand, GATA4 and Nkx2.5 together can co-activate target genes regulating cardiac development.[44] We propose that ANKRD1-mediated *GATA4* and *Nkx2.5* transcriptional modulation contributes both to cellular phenotype onset and to early abnormal venous pole remodelling, leading to SV defects (*Figure 8B*).

The extreme sensitivity to ANKRD1 levels in our Tg mice is in line with TAPVR occurrence in patients presenting a mild increase in ANKRD1 transcripts and/or protein stability.[4,21] TAPVR and SV defects present a common feature, i.e. abnormal pulmonary venous connections: PV are not connected to the left atrium in TAPVR, whereas partial anomalous PV connections characterize SV defects.[45] Our data support the hypothesis that both diseases can stem from a common developmental defect, i.e. reduced cardiac venous pole remodelling.[30,45]

The limited time-window of *GATA4-Nkx2.5* transcriptional modulation cannot account for the full, complex phenotypic spectrum of Tg mice. Dynamic titin isoform alterations in Tg hearts and reduced myofibrillar compliance accompanied by increased max force in neonatal Tg myofibrils[1,46,47] (*Figure 8B–D*), altogether indicate a correlation between increased ANKRD1 levels and titin response. Transgene expression was exclusively sarcomeric in foetal and neonatal hearts, suggesting that altered ANKRD1 stoichiometry could directly affect titin mechanosensing properties at these stages. However, as titin compliance can be finely modulated by ANKRD1 binding,[1,48] its mechanosensing properties could be affected already in early Tg embryos. We cannot additionally

rule out that ANKRD1-GATA4(-Nkx2.5)-mediated cardiomyocyte disorganization can contribute to trigger an initial titin response (*Figure 8B*). Titin can finely respond to changes in sarcomere stretch by differential splicing of its spring elements, resulting in either increased or decreased passive stiffness[40,49] and can additionally regulate sarcomere assembly[50] and stability[41] from development to adult life.[40,49,51] Thus, our data suggest that titin-mediated mechanotransduction impairment plays a relevant role in Tg cardiomyocyte phenotype functional modulation (*Figure 8B*).

Altogether, our results show that activation of *GATA4-Nkx2.5* transcription and titin gene modulation are temporally distinct but integrated systems of rapid response to changes in ANKRD1 levels and in haemodynamic load.

4.2 ANKRD1 overexpression and cardiac functional disease

Early postnatal transgenic cardiomyocytes presented signs (functional, molecular, and ultrastructural changes) of ongoing cardiac disease. They are likely the result of mechanotransduction impairment, due to changes in haemodynamic load and increased Tg expression at birth.

Disease progression in postnatal life is triggered by both the cellular/functional and the anatomical substrates. 2M Tg hearts presented an early adaptive response, likely triggered by small volume overload due to the R-L shunt and impaired compliance of ventricular cardiomyocytes (*Figure 8C*). Progressively, altered haemodynamics and impaired functionality in Tg cardiomyocytes initiate a vicious loop, that peaks to the maladaptive organ response observed at 10M (*Figure 8B*). Dramatic worsening of Tg ventricular cardiomyocyte ultrastructure in adult hearts could be caused by their altered mechanosensing properties combined to the high workload of ventricular chambers. As a support to our hypothesis, myofibrillar loss was absent in adult Tg LA, in line with its major function as a reservoir chamber.

Functional analysis demonstrated a significant slowing down in the fast component of myofibrillar relaxation kinetics in 10M Tg hearts. This finding indicates an impairment in inter-sarcomeric dynamics, likely due to the altered load conditions.[52] Comparable passive properties of 10M wt and Tg indicated that late diastolic dysfunction is due to impaired ventricular relaxation (lusitropy), not impaired passive stiffness (*Figure 8D*). Additional possible contributors to cardiomyocyte dysfunction, such as altered intracellular Ca^{2+} dynamics and impaired energetic costs[53,54] most likely contribute to the diastolic impairment.

The mechanistic links between ANKRD1 overexpression and cardiac disease progression can only partially be elucidated. However, transgene nucleo-sarcomeric sublocalization during postnatal life indicates that ANKRD1 can sense the altered cardiomyocyte status and, once a certain threshold is reached, can respond by modulating its interacting partners.

ANKRD1 gain of function mutations have been identified in HCM and DCM patients.[18,19] DCM-associated features are ventricular dilatation, wall thinning, and reduced systolic function, whereas HCM presents with normal or increased systolic function and strong variability: a subset of patients develop HF, a minority further progresses to end stage HF, which resembles DCM.[55] At the organ level, ANKRD1 Tg hearts present typical features of HCM, i.e. diastolic dysfunction with preserved systolic functionality and phenotypic variability associated to disease progression.[56] Hypertrophic response, the hallmark of human HCM disease, was not present in *ANKRD1* Tg mice, however, this is a shared characteristic of Tg mouse models of sarcomere-associated HCM mutations.[57,58]

Contractile dysfunction plays a central role in cardiomyopathies onset and progression. Increased contraction is associated to HCM onset, whereas disruption of sarcomeric function and/or structure has been suggested as early landmark of DCM.[55] ANKRD1 Tg neonatal hearts presented both features, i.e. increased myofibrils maximal force and an initial sarcomeric loss (*Figure 8C* and *D*). Cardiac disease progression is characterized by increased cardiomyocyte compliance, which is generally higher in DCM and end-stage HF, compared to early-stage patients.[59,60] In this line, the dynamic alteration of contractile properties in Tg myofibrils parallels functional changes observed in human disease.

5. Conclusions and perspectives

Our study defines for the first time a unifying picture for ANKRD1 role in heart development, CHD and adult cardiomyopathy occurrence. The complexity and multifactorial components of human disease suggests a note of caution for any direct extrapolation from animal models to humans. Phenotypic variability of our Tg mice allows to speculate that fine modulation of interacting partners and signalling pathways could result in different disease outcome in humans, as previously proposed.[61] Our results open the perspective that gain of function mutations of *ANKRD1* gene could be a prognostic early genetic marker for adult cardiomyopathy, in addition to congenital malformations, such as SV defects and TAPVR.

Supplementary material

Supplementary material is available at *Cardiovascular Research* online.

Acknowledgements

We thank Cinzia Parolini for help and support in animal handling and tissue harvesting, Walter Giuriati for histological analysis, Sandra Furlan and Marco Sandri for help in data analysis, Marta Murgia for critical reading of the manuscript and for discussion.

Conflict of interest: none declared.

Funding

This work was supported by European Union's Horizon 2020 research and innovation programme under grant agreement no. 777204 (SILICOFCM) to C.P, University of Insubria (FAR 2016-2018) and Federico Ghidoni Memorial Fund to F.A., Italian Ministry of Education, University and Research (DOR 2018) to S.A.

References

1. Lun AS, Chen J, Lange S. Probing muscle ankyrin-repeat protein (MARP) structure and function. *Anat Rec* 2014;**297**:1615–1629.
2. Miller MK, Bang M-L, Witt CC, Labeit D, Trombitas C, Watanabe K, Granzier H, McElhinny AS, Gregorio CC, Labeit S. The muscle ankyrin repeat proteins: cARP, ankrd2/Arpp and DARP as a family of titin filament-based stress response molecules. *J Mol Biol* 2003;**333**:951–964.
3. Ling SSM, Chen Y-T, Wang J, Richards AM, Liew OW. Ankyrin repeat domain 1 protein: a functionally pleiotropic protein with cardiac biomarker potential. *Int J Mol Sci* 2017;**18**:1362.
4. Badi I, Cinquetti R, Frascoli M, Parolini C, Chiesa G, Taramelli R, Acquati F. Intracellular ANKRD1 protein levels are regulated by 26S proteasome-mediated degradation. *FEBS Lett* 2009;**583**:2486–2492.
5. Zou Y, Evans S, Chen J, Kuo HC, Harvey RP, Chien KR. CARP, a cardiac ankyrin repeat protein, is downstream in the Nkx2-5 homeobox gene pathway. *Development* 1997;**124**:793–804.

6. Kuo H, Chen J, Ruiz-Lozano P, Zou Y, Nemer M, Chien KR. Control of segmental expression of the cardiac-restricted ankyrin repeat protein gene by distinct regulatory pathways in murine cardiogenesis. *Development* 1999;**126**:4223–4234.
7. Jeyaseelan R, Poizat C, Baker RK, Abdishoo S, Isterabadi LB, Lyons GE, Kedes L. A novel cardiac-restricted target for doxorubicin. CARP, a nuclear modulator of gene expression in cardiac progenitor cells and cardiomyocytes. *J Biol Chem* 1997;**272**: 22800–22808.
8. Bang ML, Mudry RE, McElhinny AS, Trombitás K, Geach AJ, Yamasaki R, Sorimachi H, Granzier H, Gregorio CC, Labeit S. Myopalladin, a novel 145-kilodalton sarcomeric protein with multiple roles in Z-disc and I-band protein assemblies. *J Cell Biol* 2001; **153**:413–427.
9. Chen B, Zhong L, Roush SF, Pentassuglia L, Peng X, Samaras S, Davidson JM, Sawyer DB, Lim CC. Disruption of a GATA4/Ankrd1 signaling axis in cardiomyocytes leads to sarcomere disarray: implications for anthracycline cardiomyopathy. Capogrossi MC, ed. *PLoS One* 2012;**7**:e35743.
10. Zhong L, Chiusa M, Cadar AG, Lin A, Samaras S, Davidson JM, Lim CC. Targeted inhibition of ANKRD1 disrupts sarcomeric ERK-GATA4 signal transduction and abrogates phenylephrine-induced cardiomyocyte hypertrophy. *Cardiovasc Res* 2015;**106**: 261–271.
11. Aihara Y, Kurabayashi M, Saito Y, Ohyama Y, Tanaka T, Takeda S, Tomaru K, Sekiguchi K, Arai M, Nakamura T, Nagai R. Cardiac ankyrin repeat protein is a novel marker of cardiac hypertrophy: role of M-CAT element within the promoter. *Hypertension* 2000;**36**:48–53.
12. Wei Y-J, Cui C-J, Huang Y-X, Zhang X-L, Zhang H, Hu S-S. Upregulated expression of cardiac ankyrin repeat protein in human failing hearts due to arrhythmogenic right ventricular cardiomyopathy. *Eur J Heart Fail* 2009;**11**:559–566.
13. Kempton A, Cefalu M, Justice C, Baich T, Derbala M, Canan B, Janssen PML, Mohler PJ, Smith SA. Altered regulation of cardiac ankyrin repeat protein in heart failure. *Heliyon* 2018;**4**:e00514.
14. Bang M-L, Gu Y, Dalton ND, Peterson KL, Chien KR, Chen J. The muscle ankyrin repeat proteins CARP, Ankrd2, and DARP are not essential for normal cardiac development and function at basal conditions and in response to pressure overload. Xu X, ed. *PLoS One* 2014;**9**:e93638.
15. Shen L, Chen C, Wei X, Li X, Luo G, Zhang J, Bin J, Huang X, Cao S, Li G, Liao Y. Overexpression of ankyrin repeat domain 1 enhances cardiomyocyte apoptosis by promoting p53 activation and mitochondrial dysfunction in rodents. *Clin Sci* 2015; **128**:665–678.
16. Song Y, Xu J, Li Y, Jia C, Ma X, Zhang L, Xie X, Zhang Y, Gao X, Zhang Y, Zhu D. Cardiac ankyrin repeat protein attenuates cardiac hypertrophy by inhibition of ERK1/2 and TGF-β signaling pathways. Hirsch E, ed. *PLoS One* 2012;**7**:e50436.
17. Arimura T, Bos JM, Sato A, Kubo T, Okamoto H, Nishi H, Harada H, Koga Y, Moulik M, Doi YL, Towbin JA, Ackerman MJ, Kimura A. Cardiac ankyrin repeat protein gene (ANKRD1) mutations in hypertrophic cardiomyopathy. *J Am Coll Cardiol* 2009;**54**: 334–342.
18. Duboscq-Bidot L, Charron P, Ruppert V, Fauchier L, Richter A, Tavazzi L, Arbustini E, Wichter T, Maisch B, Komajda M, Isnard R, Villard E; EUROGENE Heart Failure Network. Mutations in the ANKRD1 gene encoding CARP are responsible for human dilated cardiomyopathy. *Eur Heart J* 2009;**30**:2128–2136.
19. Moulik M, Vatta M, Witt SH, Arola AM, Murphy RT, McKenna WJ, Boriek AM, Oka K, Labeit S, Bowles NE, Arimura T, Kimura A, Towbin JA. ANKRD1, the gene encoding cardiac ankyrin repeat protein, is a novel dilated cardiomyopathy gene. *J Am Coll Cardiol* 2009;**54**:325–333.
20. Acquati F, Russo A, Taramelli R, Tibiletti MG, Taborelli M, Camesasca C, Papa M. Nonsyndromic total anomalous venous return associated with a de novo translocation inolving chromosomes 10 and 21 t(10; 21)(q23.1; q11.2). *Am J Med Genet* 2000; **95**:285–286.
21. Cinquetti R, Badi I, Campione M, Bortoletto E, Chiesa G, Parolini C, Camesasca C, Russo A, Taramelli R, Acquati F. Transcriptional deregulation and a missense mutation define ANKRD1 as a candidate gene for total anomalous pulmonary venous return. *Hum Mutat* 2008;**29**:468–474.
22. Correa-Villaseñor A, Ferencz C, Boughman JA, Neill CA. Total anomalous pulmonary venous return: familial and environmental factors. The Baltimore-Washington Infant Study Group. *Teratology* 1991;**44**:415–428.
23. Subramaniam A, Jones WK, Gulick J, Wert S, Neumann J, Robbins J. Tissue-specific regulation of the alpha-myosin heavy chain gene promoter in transgenic mice. *J Biol Chem* 1991;**266**:24613–24620.
24. Piroddi N, Belus A, Eiras S, Tesi C, J van der V, Poggesi C, Stienen G. No direct effect of creatine phosphate on the cross-bridge cycle in cardiac myofibrils. *Pflugers Arch* 2006;**452**:3–6.
25. Colomo F, Piroddi N, Poggesi C, G Te K, Tesi C. Active and passive forces of isolated myofibrils from cardiac and fast skeletal muscle of the frog. *J Physiol* 1997;**500**: 535–548.
26. Scellini B, Piroddi N, Flint GV, Regnier M, Poggesi C, Tesi C. Impact of tropomyosin isoform composition on fast skeletal muscle thin filament regulation and force development. *J Muscle Res Cell Motil* 2015;**36**:11–23.
27. de Lange FJ, Moorman AF, Anderson RH, Männer J, Soufan AT, de Gier-de Vries C, Schneider MD, Webb S, van den Hoff MJ, Christoffels VM. Lineage and morphogenetic analysis of the cardiac valves. *Circ Res* 2004;**95**:645–654.
28. Christoffels VM, Mommersteeg MT, Trowe MO, Prall OW, de Gier-de Vries C, Soufan AT, Bussen M, Schuster-Gossler K, Harvey RP, Moorman AF, Kispert A. Formation of the venous pole of the heart from an *Nkx2-5*-negative precursor population requires *Tbx18*. *Circ Res* 2006;**98**:1555–1563.
29. Tretter JT, Chikkabyrappa S, Spicer DE, Backer CL, Mosca RS, Anderson RH, Bhatla P. Understanding the spectrum of sinus venosus interatrial communications. *Cardiol Young* 2017;**27**:418–426.
30. G van den B, Moorman A. Development of the pulmonary vein and the systemic venous sinus: an interactive 3D overview. *PLoS One* 2011;**6**:e22055.
31. Campione M, Ros MA, Icardo JM, Piedra E, Christoffels VM, Schweickert A, Blum M, Franco D, Moorman A. Pitx2 expression defines a left cardiac lineage of cells: evidence for atrial and ventricular molecular isomerism in the iv/iv mice. *Dev Biol* 2001; **231**:252–264.
32. Hoogaars WM, Tessari A, Moorman AF, de Boer PA, Soufan AT, Campione M, Christoffels VM. The transcriptional repressor Tbx3 delineates the developing central conduction system of the heart. *Cardiovasc Res* 2004;**62**:489–499.
33. Christoffels VM, Habets PE, Franco D, Campione M, F de J, Lamers WH, Bao ZZ, Palmer S, Biben C, Harvey RP, Moorman AF. Chamber formation and morphogenesis in the developing mammalian heart. *Dev Biol* 2000;**223**:266–278.
34. Chen H, Shi S, Acosta L, Li W, Lu J, Bao S, Chen Z, Yang Z, Schneider MD, Chien KR, Conway SJ, Yoder MC, Haneline LS, Franco D, Shou W. BMP10 is essential for maintaining cardiac growth during murine cardiogenesis. *Development* 2004;**131**: 2219–2231.
35. Heldin C-H, Moustakas A. Signaling receptors for TGF-β family members. *Cold Spring Harb Perspect Biol* 2016;**8**:a022053.
36. Broberg CS, Pantely GA, Barber BJ, Mack GK, Lee K, Thigpen T, Davis LE, Sahn D, Hohimer AR. Validation of the myocardial performance index by echocardiography in mice: a noninvasive measure of left ventricular function. *J Am Soc Echocardiogr* 2003;**16**:814–823.
37. Faggiano P, Vizzardi E, Pulcini E, Maffeo D, Fracassi F, Nodari S, Dei Cas L. The study of left ventricular diastolic function by Doppler echocardiography: the essential for the clinician. *Heart Int* 2007;**3**:42.
38. Rigatelli G, Zuin M, Dell'Avvocata F. Atrial fibrillation and patent foramen potentially share same atrial flow dynamic profile and thrombotic mechanism. *Eur J Intern Med* 2017;**44**:e20–e21.
39. Linke W. Sense and stretchability: the role of titin and titin-associated proteins in myocardial stress-sensing and mechanical dysfunction. *Cardiovasc Res* 2008;**77**: 637–648.
40. Granzier HL, Labeit S. The giant protein titin. *Circ Res* 2004;**94**:284–295.
41. Linke WA, Hamdani N. Gigantic business. *Circ Res* 2014;**114**:1052–1068.
42. Gui Y-H, Linask KK, Khowsathit P, Huhta JC. Doppler echocardiography of normal and abnormal embryonic mouse heart. *Pediatr Res* 1996;**40**:633–642.
43. Brewer AC, Alexandrovich A, Mjaatvedt CH, Shah AM, Patient RK, Pizzey JA. GATA factors lie upstream of Nkx 2.5 in the transcriptional regulatory cascade that effects cardiogenesis. *Stem Cells Dev* 2005;**14**:425–439.
44. McCulley DJ, Black BL. Transcription factor pathways and congenital heart disease. *Curr Top Dev Biol* 2012;253–277.
45. Butts RJ, Crean AM, Hlavacek AM, Spicer DE, Cook AC, Oechslin EN, Anderson RH. Veno-venous bridges: the forerunners of the sinus venosus defect. *Cardiol Young* 2011;**21**:623–630.
46. Elhamine F, Radke MH, Pfitzer G, Granzier H, Gotthardt M, Stehle R. Deletion of the titin N2B region accelerates myofibrillar force development but does not alter relaxation kinetics. *J Cell Sci* 2014;**127**:3666–3674.
47. Sequeira V, Velden J. V D. The Frank–Starling Law: a jigsaw of titin proportions. *Biophys Rev* 2017;**9**:259–267.
48. Zhou T, Fleming JR, Franke B, Bogomolovas J, Barsukov I, Rigden DJ, Labeit S, Mayans O. CARP interacts with titin at a unique helical N2A sequence and at the domain Ig81 to form a structured complex. *FEBS Lett* 2016;**590**:3098–3110.
49. Anderson BR, Granzier HL. Titin-based tension in the cardiac sarcomere: molecular origin and physiological adaptations. *Prog Biophys Mol Biol* 2012;**110**: 204–217.
50. Walker JS, Tombe PP. D. Titin and the developing heart. *Circ Res* 2004;**94**:860–862.
51. Opitz CA, Leake MC, Makarenko I, Benes V, Linke WA. Developmentally regulated switching of titin size alters myofibrillar stiffness in the perinatal heart. *Circ Res* 2004; **94**:967–975.
52. Poggesi C, Tesi C, Stehle R. Sarcomeric determinants of striated muscle relaxation kinetics. *Pflugers Arch* 2005;**449**:505–517.
53. Borlaug BA, Kass DA. Mechanisms of diastolic dysfunction in heart failure. *Trends Cardiovasc Med* 2006;**16**:273–279.
54. Lopes LR, Elliott PM. A straightforward guide to the sarcomeric basis of cardiomyopathies. *Heart* 2014;**100**:1916–1923.
55. Garfinkel AC, Seidman JG, Seidman CE. Genetic pathogenesis of hypertrophic and dilated cardiomyopathy. *Heart Fail Clin* 2018;**14**:139–146.
56. J van der V, Ho CY, Tardiff JC, Olivotto I, Knollmann BC, Carrier L. Research priorities in sarcomeric cardiomyopathies. *Cardiovasc Res* 2015;**105**:449–456.
57. Moore RK, Grinspan LT, Jimenez J, Guinto PJ, Ertz-Berger B, Tardiff JC. HCM-linked Δ160E cardiac troponin T mutation causes unique progressive structural and molecular ventricular remodeling in transgenic mice. *J Mol Cell Cardiol* 2013;**58**:188–198.

58. Michele DE, Gomez CA, Hong KE, Westfall MV, Metzger JM. Cardiac dysfunction in hypertrophic cardiomyopathy mutant tropomyosin mice is transgene-dependent, hypertrophy-independent, and improved by beta-blockade. *Circ Res* 2002;**91**:255–262.
59. van Heerebeek L, Borbély A, Niessen HW, Bronzwaer JG, van der Velden J, Stienen GJ, Linke WA, Laarman GJ, Paulus WJ. Myocardial structure and function differ in systolic and diastolic heart failure. *Circulation* 2006;**113**:1966–1973.
60. Vikhorev P, Vikhoreva N. Cardiomyopathies and related changes in contractility of human heart muscle. *Int J Mol Sci* 2018;**19**:2234.
61. Lange S, Gehmlich K, Lun AS, Blondelle J, Hooper C, Dalton ND, Alvarez EA, Zhang X, Bang M-L, Abassi YA, Remedios CD, Peterson KL, Chen J, Ehler E. MLP and CARP are linked to chronic PKCα signalling in dilated cardiomyopathy. *Nat Commun* 2016;**7**:12120.

Translational perspective

Increased ANKRD1 levels linked to gain of function mutations have been correlated to total anomalous pulmonary venous return (TAPVR) and adult cardiomyopathy in humans. Myocardial-overexpressing ANKRD1 mouse lines are born with congenital sinus venosus (SV) defect and progressively develop diastolic dysfunction with preserved EF, which evolves into heart failure. Our data indicate that impaired embryonic remodelling and adult heart dysfunction stem from a common ground of initial cardiomyocyte defects, which are exacerbated postnatally. Our results open the perspective that gain of function mutations of *ANKRD1* gene could be a prognostic early genetic marker for adult cardiomyopathy, in addition to selective congenital malformations such as SV defects and TAPVR.